AUGUST 01 2009

A note on noise propagation in street canyons

Kai Ming Li; Chenly Yuen Cheung Lai

J. Acoust. Soc. Am. 126, 644–655 (2009)
https://doi.org/10.1121/1.3158599

A note on noise propagation in street canyons

Kai Ming Li
Ray W. Herrick Laboratories, School of Mechanical Engineering, Purdue University, 140 South Martin Jischke Drive, West Lafayette, Indiana 47907-2031

Chenly Yuen Cheung Lai
Department of Mechanical Engineering, The Hong Kong Polytechnic University, Hung Hom, Kowloon, Hong Kong

(Received 15 November 2008; revised 12 May 2009; accepted 13 May 2009)

The current study examines the propagation of sound in street canyons with geometrically reflecting surfaces. An image source method is a popular numerical model to estimate the propagation of sound energy in a street canyon. This numerical model calculates the total sound energy received at a field point by summing the contributions from individual image sources incoherently. The discrete image source model is generalized by replacing rows of point sources with their respective line sources. An integral formulation is derived, which can be evaluated exactly to give a simple analytical solution. The expression permits rapid computations of the sound energy due to a point source placed in a street canyon. The transient sound energy at a receiver point is also examined. It has been demonstrated that the transient sound energy can be expressed in terms of a standard exponential integral. The Schroeder integration method is then used to calculate the reverberation times, which allow a straightforward assessment of the acoustic environment in street canyons. Indoor and outdoor experiments were conducted to validate the proposed integral formulation. The analytical formulas were also compared with numerical results based on the standard image source method and with published experimental data. © *2009 Acoustical Society of America.*
[DOI: 10.1121/1.3158599]

PACS number(s): 43.50.Rq, 43.50.Gf, 43.55.Dt, 43.55.Br [NX] Pages: 644–655

I. INTRODUCTION

In the past few decades, we witnessed a rapid growth in mechanized transport and transportation systems. Noise is one of the most cited environmental factors that are most commonly associated with pollution from transport. Various modes of land transportation are the primary source of noise in dense, high-rise cities. An essential feature of compact and high-rise cities is that the scarcity of suitable land has encouraged building development to go up in the vertical dimension. It is common to find residential and commercial tower blocks of over 40 storeys with height over 100 m or even more. Worse still, the urban areas are typically embedded with a compact traffic network of highways and/or railways with high traffic volume. The lack of available land space means that the residents are closer to noise sources. The tall flanking buildings, which form a street canyon, permit large portion of the dwellings exposing to the land transportation noise. The noise levels do not decrease significantly with the height above the ground in street canyons.[1–4] The motivation of the current study is to develop a simple formula to evaluate steady-state noise levels and the reverberation times in a street canyon for assessing the effectiveness of noise control.

It is of interest to point out that the first measurements of sound propagation in urban area were performed to determine an optimal location for sirens during 1940s.[5,6] Wiener *et al.*[7] conducted a theoretical study on the propagation of sound, the reverberation time, and speech intelligibility in a city street of Boston. In 1970s, Aylor *et al.*[8] conducted a study to investigate the effect of ivy grown on building façades on the reverberation time. Yeow[9,10] performed some measurements of the reverberation time in downtown residential areas. From their experimental results, Ko and Tang[11] suggested that the reverberation time of a street canyon was proportional to the volume bounded by the tall buildings in street canyons. Steenackers *et al.*[12] carried out a series of experimental measurements of the sound decay curves in a street canyon. Their study was focused on the determination of the absorption coefficient in favor of the reverberation time of the street canyons but no theoretical models were offered.

There were also a number of other studies addressing the theoretical and numerical aspects of sound propagation in street canyons in the past few decades. Typically, either an image source model or a diffuse reflection model is used to compute the sound fields and the reverberation times in a street canyon.[13–16] Most of the image source methods are based on incoherent model[17] although a coherent model has been used in a recent study.[18] Despite these theoretical and experimental studies, there is still no simple but accurate formula to predict the noise levels and the reverberation time in street canyons. The present study is aimed to develop such a simple but accurate analytical expression to predict the noise levels and to calculate the reverberation time rapidly. This, in turn, allows the assessment of the acoustic treatments in street canyons.

We remark that the scattering of sound at the façade surfaces is known to be significant for predicting the transmission of noise along a street canyon.[13,14] We shall use the

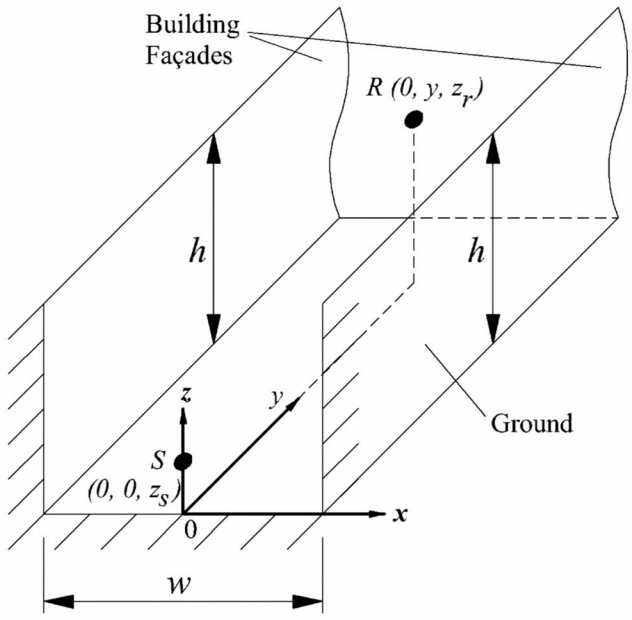

FIG. 1. Schematic showing the rectangular coordinate system and the geometrical configuration of a street canyon.

image source model where the boundaries can be taken as smooth, geometrically reflecting surfaces in the present study. It is because this model is simple yet it can be used to represent some urban situations. The closed-form analytical results can be used to offer a first order engineering approximation to supplement the numerical results obtained from other computational intensive schemes, e.g., the diffuse reflection model.[15,16]

The paper is arranged as follows. Section II presents an integral formulation to calculate the noise levels and the reverberation times in street canyons. In Sec. III, the theoretical models are validated by comparing the numerical predictions with experimental results. Section III A shows comparisons of numerical results with published experimental data.[12] In Sec. III B and III C, we present indoor and outdoor experimental results. These measured results are compared with the numerical predictions based on the integral formulations. The outcomes of the present study are summarized in Sec. IV.

II. THEORY

A. Total steady-state sound energy at a receiver

A street canyon may be considered as a category of a long enclosure: The flanking façades are treated as a pair of parallel side walls, the road pavement is taken as the floor, and the opening at the top is represented by a perfectly absorptive ceiling. Taking the boundaries as geometrically reflecting surfaces, the sound propagation along the street canyon can be calculated by means of an image source method.[16] Figure 1 displays an idealized street canyon where h is the height of the buildings measured in the z-direction. The pair of flanking façade surfaces is parallel to each other with a horizontal separation of w measured in the x-direction. The y-axis is aligned along the direction of the street canyon. The origin is located on the ground at equidistance from the parallel flanking buildings where the façade surfaces are situated at $x=\pm w/2$.[19]

In the current study, we consider a typical situation where the height of the flanking façades is greater than the width of the street canyon, i.e., $h>w$. The effect of diffraction at the top edges of the façades is ignored in the present study. It is because the total sound energy at a receiver point is dominated by the contributions from multiple reflected sound rays of the boundary surfaces. In general, the noise levels due to vehicular noise sources decrease with an increase in the receiver height because there are no reflections from the open ceiling of the street canyon. In addition, the noise levels decrease with the increase in the separation between the source and receiver along the y-direction. However, Kang[16] showed that the noise levels are relatively uniform between the buildings for a fixed horizontal separation (greater than about $1.5w$) from the source and at a constant height above the ground. Without loss of generality, we therefore assume that a point source S and a receiver R are located at the coordinates of $(0,0,z_s)$ and $(0,y,z_r)$, respectively. Hence, the sound source is separated from the receiver by a horizontal distance

$$r_I=\sqrt{y^2+(z_r-z_s)^2}. \tag{1}$$

A row of image sources, shown as the upper row in Fig. 2, is formed because of the reflections from the two vertical façade surfaces. Based on this series of image sources, the lower row of image sources can be constructed below the $z=0$ plane due to the reflection from the ground surface. All image sources can be linked to the receiver and the total sound field is computed by summing the contributions from these image sources. Making use of the image source model, the total sound energy at the receiver due to the image sources located above the ground is given by

$$\Lambda_I=\sum_{m=-\infty}^{\infty}\frac{Qe^{m\ln(1-\bar{\alpha}_v)-\alpha_a d_m}}{d_m^2}, \tag{2}$$

where Q is the source strength, $\bar{\alpha}_v$ is the mean absorption coefficient of the façade surfaces, and α_a is the air absorption factor, which can be obtained from Ref. 20 for different frequencies. The path length of the $\pm m$th image source can be determined by

$$d_m=\sqrt{(mw)^2+r_I^2}, \tag{3}$$

where r_I is determined according to Eq. (1). Here, in Eq. (2), the attenuation due to the reflection from the boundary surfaces is written in its exponential form by noting the following algebraic identity:

$$e^{m\ln(1-\bar{\alpha}_v)}=(1-\bar{\alpha}_v)^m, \tag{4}$$

where $\ln(1-\bar{\alpha}_v)<0$ because $\bar{\alpha}_v<1$ and m is the number of reflections from the façades.

Suppose that the façades are built with hard surfaces with small $\bar{\alpha}_v$. In this case, the total sound energy received at the reception point is composed of many terms due to the multiple reflections from the façade surfaces. It is possible to replace m with a continuous function in terms of x as

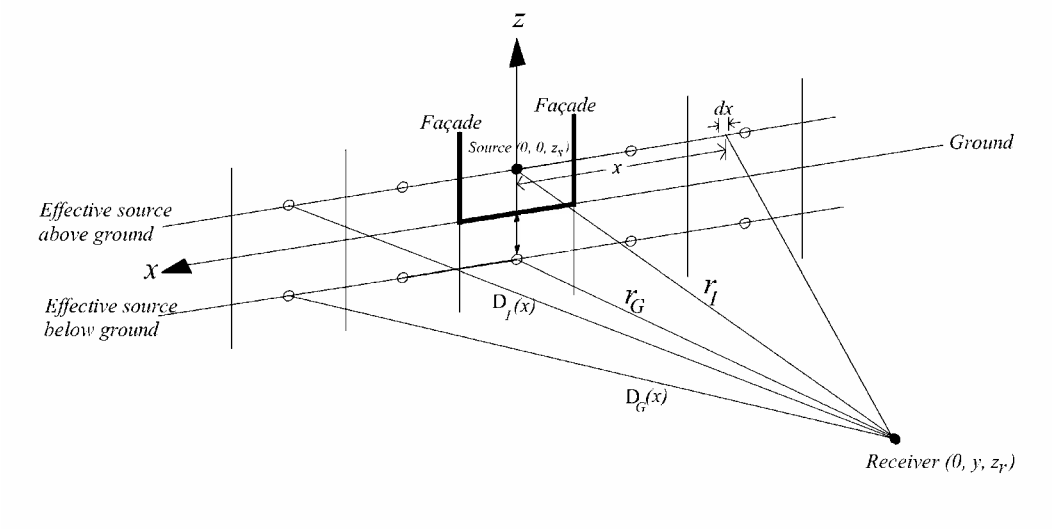

FIG. 2. Schematic to show the relative locations of the receiver, the point source (solid circle), image sources (open circle), and the corresponding line sources above and below the ground surface.

$$m = |x|/w. \tag{5}$$

A line source can now be used to replace the upper row of the discrete image sources. Figure 2 shows a schematic of the effective line source. It has an effective strength of Q/w m^{-1} because there is only one image source for the width, w, of the street canyon. The path length d_m can be replaced with

$$D_I = \sqrt{x^2 + r_I^2}. \tag{6}$$

From Eq. (2), the sound energy at the reception point due to the image sources above the ground can be written in an integral form as

$$\Lambda_I = \frac{\Lambda_0}{w}\int_0^\infty \Phi_I dx, \tag{7}$$

where Φ_I is a symmetric function of x given by

$$\Phi_I = \Phi_I(x) = \frac{2e^{\{x\ln(1-\bar{\alpha}_v)/w - \alpha_a D_I\}}}{D_I^2}, \tag{8}$$

and Λ_0 is the free-field sound energy received at a distance of 1 m from the point source. It can be determined by

$$\Lambda_0 = Qe^{-\alpha_a(1)}/1^2 \approx Q. \tag{9}$$

The integral in Eq. (7) is difficult, if not impossible, to evaluate analytically because of the presence of D_I in the exponential term of $\Phi_I(x)$. Although the integral can be evaluated by a numerical quadrature, it is more convenient to approximate the solution in an analytical form.

To this end, we approximate D_I in the exponential term of Eq. (9) by a linear function

$$D_I = \sqrt{r_I^2 + x^2} \approx r_I + K_I x, \tag{10}$$

where K_I is the slope of the approximate function. Since the solution is given in an integral form [cf. Eqs. (7) and (8)], it is convenient to approximate K_I such that

$$\int_0^{X_I} \sqrt{r_I^2 + x^2}\,dx = \int_0^{X_I} (r_I + K_I x)dx, \tag{11}$$

where the upper limit of the integrand, X_I, is set at a sufficiently large distance in order to cover the range of x that contributes to the total sound energy at the reception point. As $\Phi_I(x)$ is a monotonic decreasing function, we can approximate X_I by the following function:

$$\varepsilon = \Phi_I(X_I)/\Phi_I(0), \tag{12}$$

where ε is the ratio of the minimum sound energy and the maximum sound energy contributed due to the effective line source. The minimum sound energy is contributed from a source located at $x = X_I$ and the maximum contribution comes from the source located at $x = 0$. Preliminary numerical analyses have suggested that the predicted results are relatively the same for a wide range of ε. Hence, for simplicity, ε is chosen as 1×10^{-6} in the following numerical analyses.

It is remarkable that both integrals in Eq. (11) can be evaluated analytically to give closed-form expressions. As a result, K_I can be written in an analytical form to yield

$$K_I = \frac{2}{X_I^2}\left\{\frac{r_I^2}{2}\left[\ln\left(\frac{X_I + \sqrt{r_I^2 + X_I^2}}{r_I}\right) + \frac{X_I\sqrt{r_I^2 + X_I^2}}{r_I^2}\right] - r_I X_I\right\}. \tag{13}$$

Substituting Eqs. (8), (10), and (13) into Eq. (7), we can approximate Λ_I by

$$\Lambda_I \approx \frac{2\Lambda_0 e^{-\alpha_a r_I}}{w}\int_0^\infty \frac{e^{-\upsilon_I x}}{r_I^2 + x^2}dx, \tag{14}$$

where

$$\upsilon_I = -\ln(1 - \bar{\alpha}_v)/w + \alpha_a K_I. \tag{15}$$

By using the following identity of an indefinite integral for the exponential integral:[21]

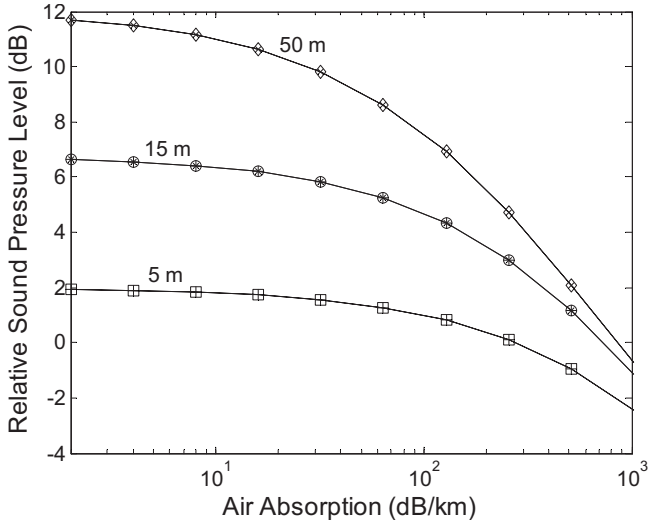

FIG. 3. The relative SPL is plotted versus the absorption factor in air. The squares, circles, and diamonds are the numerical results based on the direct numerical integration of Eq. (7) for the source/receiver separations of 5, 15, and 50 m, respectively. The plus, asterisks, and crosses are the corresponding results based on the approximate formula given in Eq. (17). The source and receiver are located at the center line of the street canyon and at the same height above the ground. The reference SPL is taken as 1 m free-field SPL; see Eq. (18).

$$\int \frac{e^x}{a^2+x^2}dx = -\frac{1}{a}\mathrm{Im}\{e^{ia}E_1(-x+ia)\} + \mathrm{const}, \tag{16}$$

we can simplify Eq. (14) to yield

$$\Lambda_I \approx \frac{-2\Lambda_0 e^{-\alpha_a r_I}}{w r_I}\mathrm{Im}[e^{i\upsilon_I r_I}E_1(i\upsilon_I r_I)], \tag{17}$$

where E_1 is the exponential integral with complex arguments.

We demonstrate the accuracy of Eq. (17) by comparing the numerical results obtained by direct numerical integration of Eq. (7). Figure 3 shows comparisons of these two numerical results in which the relative sound pressure level (SPL) is plotted against the air absorption factor α_a. In the plots, the relative SPL is defined as

$$\mathrm{SPL}_r = 10\log(\Lambda_I/\Lambda_0), \tag{18}$$

where Λ_0 is the free-field sound energy at 1 m from the source. In Fig. 3, a street canyon of 3 m wide and 100 m high is used in the numerical calculations. We assume that the building façades are perfectly reflecting surfaces, i.e., $\bar{\alpha}_v=0$. Numerical results with the horizontal separation between the source and receiver of 5, 15, and 50 m, respectively, are shown. Both source and receiver are located at equidistance from façades and at the same height above the ground. It follows from Fig. 3 that the numerical results according to both schemes agree very well with each other. These comparisons have demonstrated the accuracy of the approximate model, which is sufficient to estimate the effect of the atmospheric absorption in a street canyon of typical source/receiver geometrical configurations.

Similarly, we can derive an analogous expression for the sound energy due to the image sources located below the ground as follows:

$$\Lambda_G = \frac{\Lambda_0 e^{-\alpha_a r_G}}{w}\int_0^\infty \Phi_G dx, \tag{19}$$

where the subscript G denotes the corresponding parameters for the ground-reflected waves. The symmetric function $\Phi_G(x)$ is given by

$$\Phi_G = \Phi_G(x) = \frac{2(1-\alpha_G)e^{\{x\ln(1-\bar{\alpha}_v)/w-\alpha_a D_G\}}}{D_G^2}, \tag{20}$$

where α_G is the absorption coefficient of the ground, D_G is the total distance between the receiver and the image sources below the ground

$$D_G = \sqrt{x^2+r_G^2}, \tag{21}$$

and r_G is the corresponding horizontal separation

$$r_G = \sqrt{y^2+(z_r+z_s)^2}. \tag{22}$$

Using an analogous approach, we can derive an approximate expression for the sound energy at the reception point due to the image sources below the ground as follows:

$$\Lambda_G = \frac{-2\Lambda_0(1-\alpha_G)e^{-\alpha_a r_G}}{w r_G}\mathrm{Im}[e^{i\upsilon_G r_G}E_1(i\upsilon_G r_G)], \tag{23}$$

where the parameters υ_G and K_G are given by

$$\upsilon_G = -\ln(1-\overline{\alpha_v})/w + \alpha_a K_G \tag{24a}$$

and

$$K_G = \frac{2}{X_G^2}\left\{\frac{r_G^2}{2}\left[\ln\left(\frac{X_G+\sqrt{r_G^2+X_G^2}}{r_G}\right)+\frac{X_I\sqrt{r_G^2+X_G^2}}{r_G^2}\right] - r_G X_G\right\}. \tag{24b}$$

By means of the same approach, it is possible to determine X_G by solving an analogous equation [cf. Eq. (11)] numerically. However, it is remarkable that the same term (i.e., X_G=X_I) may also be used in Eq. (24b) for calculating K_G. A numerical analysis has suggested that a small variation in X_G does not cause a significant change in the numerical values of Λ_G. The details of these numerical analyses are not shown here for brevity.

The total sound energy can now be found by summing the contributions from all image sources (above and below the ground) to give

$$\Lambda_T = \Lambda_I + \Lambda_G, \tag{25}$$

where Λ_I and Λ_G are determined by Eqs. (7) and (19), respectively. It is possible to give a closed-form solution for Λ_T by substituting Eqs. (17) and (23) into Eq. (25) to yield

$$\Lambda_T = \frac{-2\Lambda_0 e^{-\alpha_a r_I}}{w r_I}\mathrm{Im}[e^{i\upsilon_I r_I}E_1(i\upsilon_I r_I) + A_G(1-\alpha_G)e^{i\upsilon_G r_G}E_1(i\upsilon_G r_G)], \tag{26}$$

where A_G is a correction factor for the change in distances because the image sources are located below the ground. It is given by

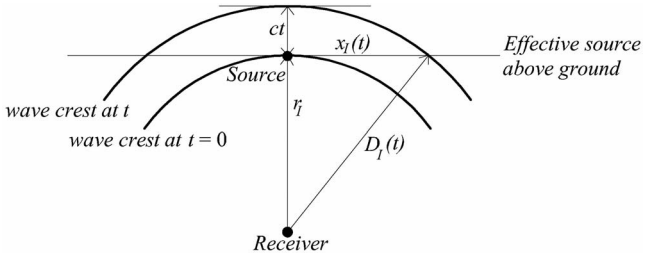

FIG. 4. Schematic to show the wave crests centering at the receiver at time $t=0$ and at time t.

$$A_G = (r_I/r_G)e^{-\alpha_a(r_G-r_I)}. \tag{27}$$

If the source is located near the ground and at a large horizontal separation from the receiver (i.e., $r_I \approx r_G$), A_G is approximately equal to unity.

B. Reverberation time in street canyons

To assess the effect of multiple reflections, it is useful to determine the reverberation times in a street canyon. The problem may be treated as the determination of the transient sound field when the source is either switched on or turned off. According to the principle of reciprocity, we may consider the receiver as the center of the wave fronts: the crests of spherical waves radiating from the receiver, which arrive at different image sources at different times. For convenience, the initial time $t=0$ is set at the moment when the direct sound wave reaches the receiver R. Suppose that the source is turned on at time $t=-r_I/c$. Then the position of a wave crest at time $t>0$ is located at a horizontal distance $x_I(t)$ from the source S. By a simple geometrical consideration, the path length D_I from the receiver to an image source above the ground can be determined by

$$D_I(t) = \sqrt{x_I(t)^2 + r_I^2} = r_I + ct, \tag{28}$$

where r_I is given by Eq. (1); see Fig. 4 for a schematic of the wave crests at time $t=0$ and at time t.

According to Eq. (14), the transient sound energy due to the image sources above the ground can then be written as

$$\Gamma_I(t) = \frac{2\Lambda_0 e^{-\alpha_a r_I}}{w}\int_0^{x_I(t)} \frac{e^{-\upsilon_I x}}{r_I^2 + x^2}dx, \quad t>0, \tag{29}$$

since only those sources located in the region $-x_I(t) \le x \le x_I(t)$ can contribute to the sound field at the reception point. Equation (29) can be reduced to Eq. (14) when $t\to\infty$, i.e., the total transient sound energy $\Gamma_I(\infty)$ becomes the steady-state sound energy at the reception point.

We can also consider a complimentary situation when the source is originally turned on but it is deactivated at $t=-r_I/c$ where c is the sound speed in air. In this case, the transient sound energy at time t is simply given by

$$\Gamma_I^*(t) = \frac{2\Lambda_0 e^{-\alpha_a r_I}}{w}\int_{x_I(t)}^{\infty} \frac{e^{-\upsilon_I x}}{r_I^2 + x^2}dx, \quad t>0. \tag{30}$$

The integrals given in Eqs. (30) and (29) can be evaluated, respectively, to yield

$$\Gamma_I^*(t) = -\frac{2\Lambda_0 e^{-\alpha_a r_I}}{wr_I}\mathrm{Im}\{e^{i\upsilon_I r_I}E_1[\upsilon_I(x_I + ir_I)]\} \tag{31}$$

and

$$\Gamma_I(t) = \Lambda_I - \Gamma_I^*(t), \tag{32}$$

where Λ_I is determined from Eq. (17).

Similarly, the transient sound energy due to the image source located below the ground can be determined when the source is turned off at $t=-r_I/c$. However, the sound energy starts to decay at a later time at $t=(r_G/r_I)/c$ because r_G/r_I. The transient sound energy is given by

$$\Gamma_G^*(t) = -\frac{2\Lambda_0 e^{-\alpha_a r_G}}{wr_G}\mathrm{Im}\{e^{i\upsilon_G r_G}E_1[\upsilon_G(x_G + ir_G)]\}, \quad t \ge (r_G - r_I)/c, \tag{33}$$

where x_G is determined by the following equation:

$$D_G(t) = \sqrt{x_G(t)^2 + r_G^2} = r_G + ct. \tag{34}$$

On the other hand, if the source is activated at $t=0$, then the transient sound energy is given by

$$\Gamma_G(t) = \Lambda_G - \Gamma_G^*(t), \quad t \ge (r_G - r_I)/c. \tag{35}$$

The effect of multiple reflections on street canyons can be assessed by considering the reverberation times, T_{60} and T_{30}, where T_{60} is the time for the noise level to reduce by 60 dB below the initial level and T_{30} is the decay time for the noise level to drop from -5 to -35 dB. A decay curve in the noise level is normally needed to determine T_{60} and T_{30}. Therefore, we focus on the transient sound energy when the source is turned off in favor of the transient sound energy when the source is activated. The total transient sound energy can be obtained by summing the contributions from the image sources located above and below the ground. From Eqs. (31) and (33), we can obtain

$$\begin{aligned}\Gamma_T^*(t) &= \Gamma_I^*(t) + \Gamma_G^*(t) \\ &= -\frac{2\Lambda_0 e^{-\alpha_a r_I}}{wr_I}\mathrm{Im}\{e^{i\upsilon_I r_I}E_1[\upsilon_I(x_I + ir_I)] \\ &\quad + A_G(1-\alpha_G)e^{i\upsilon_G r_G}E_1[\upsilon_G(x_G + ir_G)]\}.\end{aligned} \tag{36}$$

Since the current formulation is based on the image source method, it is important to demonstrate the validity of the model by comparing the current numerical results with those predicted by the image source model. It is sufficient to show plots of the decay curves with the source turned off at $t=r_I/c$. Figure 5 displays these comparisons at different mean absorption coefficients of all boundary surfaces of 0.15, 0.2, 0.25, and 0.3, respectively. The width of 10 m and the source/receiver separation of 10 m are used in the calculations. In the graphs, the relative SPLs are defined as

$$L(t) = 10\log[\Gamma_T^*(t)/\Gamma_T^*(0)], \tag{37}$$

where the reference level $\Gamma_T^*(0)$ is taken as the initial noise level. The source and receiver are placed, respectively, at 0.5 and 5.0 m above the ground and they are located at equidistance from the façade surfaces. We can see from Fig. 5 that the predicted decay curves according to the image source

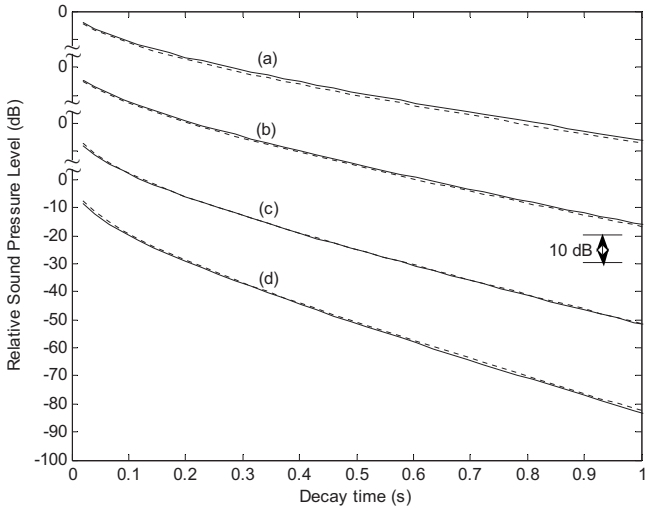

FIG. 5. The relative SPL is plotted versus time in a street canyon with the width of 10 m, and the source/receiver separation of 10 m. The source and receiver are placed, respectively, at 0.5 m and receiver at 5 m above the ground and they are located at equidistance from the façade surfaces. The mean absorption coefficients of all boundary surfaces are the same at (a) 0.15, (b) 0.2, (c) 0.25, and (d) 0.3. The solid lines (——) are the predictions by the integral formulation and the dotted lines (-----) are the predictions by the image source method. The reference SPL is taken at the initial time when the source is turned off; see Eq. (37).

method and the integral formulation agree tolerably well with each other in all cases.

Using Eq. (36), the decay curve can be produced by a reverse-time integration of the transient response. This process is known as the Schroeder approach.[22,23] The reverberation time T_{60} is then determined by using the rate of decay given by the linear regression with the noise level reducing by 60 dB from the initial level. In other words, T_{60} can be determined for the time when the ratio of $\Gamma_T^*(t)/\Gamma_T^*(0)$ is reduced to 10^{-6}. If the reverberation time T_{30} is required, Eq. (37) will be used to obtain the decay curve. A linear regression analysis is conducted to determine the rate of decay for the noise level varying between 5 and 35 dB below $\Gamma_T^*(0)$.

III. COMPARISON WITH EXPERIMENTAL MEASUREMENTS

A. Full scale field measurements in a town street

In the 1970s, Steenackers *et al.*[12] carried out a series of measurements for the reverberation time of typical town streets with their widths varying between 9 and 60 m. An alarm gun was used as an impulsive noise source where the sound decay curves were measured. The reverberation time was then used to estimate the sound absorption coefficient of the town street. Their experimental data[12] will be used to validate the integral expression given in Eq. (36). We also compare the numerical results based on the image source model with geometrically reflected boundary surfaces.[16]

Figure 6 displays the measured time histories of the relative SPLs adapted from the published data.[12] They were the sound level decay curves in the town streets with the respective widths of 12, 18, and 40 m. The horizontal distances between the source and receiver for all measurements, which were estimated from the experimental data, were 10 m. Since the exact locations of the source and receiver are not available in Ref. 12, we assume that they were placed at 1.2 m above the ground and at equidistance from the flanking buildings.

To confirm the validity of this assumption, a prior numerical analysis is conducted to examine the effect of the source location on the SPLs at different receiver locations along the street canyon. It is found that the sound fields are generally uniform within the same cross sections of the street canyon, especially, when the source and receiver are close to the ground and their horizontal separation is sufficiently

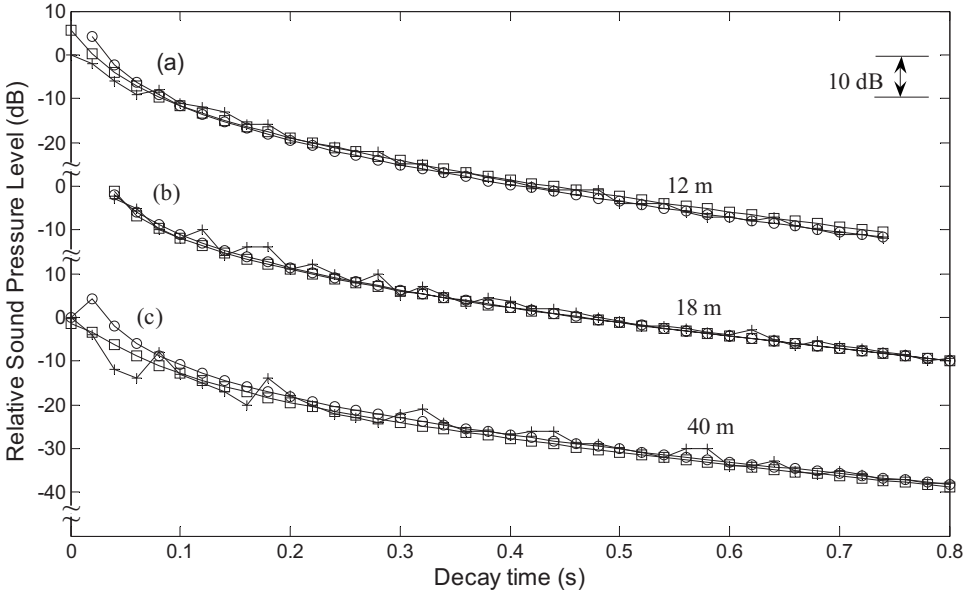

FIG. 6. The relative SPL is plotted versus time in town streets with the source/receiver separation of 10 m and the source and receiver were located at 1.2 m above the ground. The widths of the town street are (a) 12, (b) 18, and (c) 40 m. The lines with plus signs (+) are measurement results taken from Ref. 12. The lines with squares (□) are predictions by the integral formulation. The lines with circles (○) are predictions by the image source method. The reference SPL is taken at the initial time when the source is turned off; see Eq. (37).

large. These numerical simulations are not shown here but this finding is in agreement with the conclusion suggested by Kang.[16] With these prior numerical simulations, we expect that their assumption on the source/receiver locations will be sufficient to give accurate predictions of the sound fields in the street canyons.

In addition to the published data, Fig. 6 also presents the numerical predictions according to the image source model[16] and the current formulation. In his numerical analyses, Kang[16] also used the incoherent model but he computed the overall SPL by summing the contributions from all image sources, which have been "switched" on. The number of image sources increases discretely to its steady-state level after the first arrival of the direct wave. The number of "switched-on" image sources reaches its maximum level after a short duration. Hence, the image source model predicts a step change in the sound energy level shortly after the first arrival time but time-varying sound energy will gradually become the steady-state level as the time increases.

In the numerical calculations of all town streets, we assume that the air absorption factor is zero because no pertinent information is provided for the atmospheric conditions during the measurement periods. In Fig. 6(a), we present the predicted and measured results for the town street of 12 m wide. According to Steenackers *et al.*,[12] the ground was assumed to be a perfectly reflecting surface and the average mean absorption coefficient of the building façades was 0.15. For the given source and receiver locations, Eq. (37) is used to evaluate the time history of the relative SPLs. The numerical predictions according to the image source model and the integral formulation agree to within 1.1 dB in the relative SPL. Furthermore, both predicted results show good agreements with the experimental data.

Figure 6(b) presents a set of data taken from Fig. 1 of Ref. 12 where the width of the town street was 18 m. The estimated sound absorption coefficient, which was taken from Table I of Ref. 12, was 0.17. Again, we use Eq. (37) to calculate the time histories of the relative SPLs. The average discrepancy between the measured data and the image source model is 1.21 dB while it is 1.15 dB for the integral formulation.

The compared results for the last set of data are displayed in Fig. 6(c). Based on the information obtained from Steenackers *et al.*,[12] we estimated that the mean absorption coefficient of the façade was 0.3. Figure 6(c) shows tolerably good agreements between the measured data and the numerical results according to both prediction methods. The average discrepancies between the image source method and measured results are 1.54 and 1.35 dB for that of the integral formulation.

By comparing with published experimental data, it is enlightening to confirm the validity of the analytical formulation for predicting the relative SPL in a street canyon. The proposed model provides a simple closed-form solution, which compares well with the standard image source model and with the published experimental results.

FIG. 7. (Color online) Photograph showing the setup of the indoor experiment conducted in an anechoic chamber.

B. Indoor model experiments

A model street canyon was built and placed in an anechoic chamber of internal dimensions of $6\times6\times4$ m^3 (high). Hard plywood boards of 20 mm thickness were used to construct the model street canyon of 0.8 m wide, 5 m long, and 2.6 m high. The hard plywood boards were varnished to prevent leakage of sound. To simulate the façade surfaces with finite impedance, the two vertical walls were covered with acrylic light diffusers of 5 mm thickness; see Fig. 7. The light diffusers have rectangular grids with dimensions of 15×15 mm^2 and open volumes. The light diffusers may give diffused sound fields but, nevertheless, Daigle *et al.*[24] demonstrated experimentally that a hard ground covered with light diffusers can be used to simulate an indoor impedance plane. In light of the suggestion of Daigle *et al.*,[24] we conducted a set of short-range measurements for the propagation of sound above the hard plywood board covered with and without light diffusers. In these measurements, the source and receiver were placed at a horizontal separation of 1 m and at heights of 0.01 m above the model ground.

Figure 8(a) shows a typical measured spectrum to demonstrate the interference effects due to the direct and reflected waves for sound propagation above the model impedance ground. The excess attenuation, which is defined as the ratio of the total field above the impedance surface to the free-field measurement at 1 m in the anechoic chamber, is plotted against the source frequency in Fig. 8(a). We also conducted similar measurements for the propagation of sound over the hard plywood board. Its measured excess

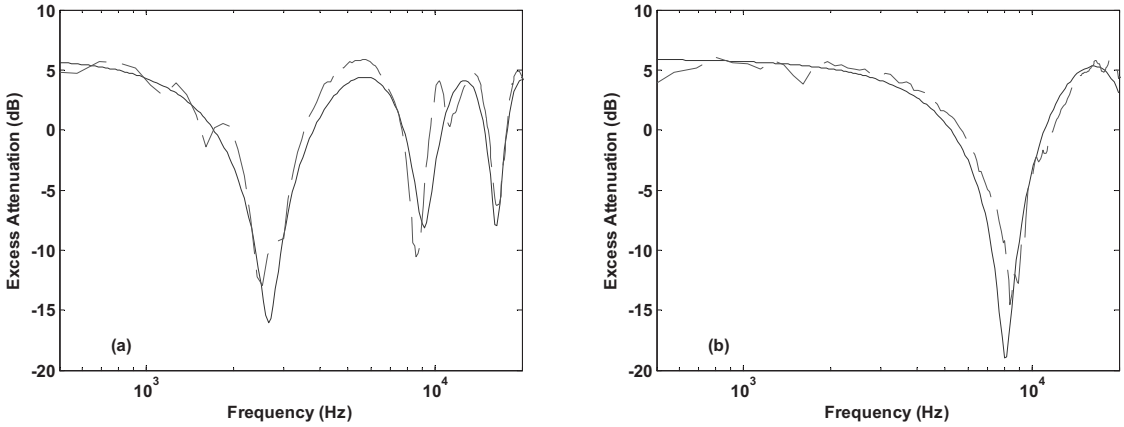

FIG. 8. The acoustic characterization of (a) the vertical walls (indoor façades) and (b) the hard floor (indoor ground). The two-parameter model was used to characterize the surface impedances. These parametric values are listed in Table I for information. The solid lines are (——) are theoretical predictions and the dotted lines (----) are experimental data.

attenuation spectrum is shown in Fig. 8(b). From both graphs in Fig. 8, there are clear interference dips due to the interference of the direct and reflected waves although the primary dip occurs at higher frequency for the hard ground. It is because the impedance of a hard surface is usually higher than that of the model plane with finite impedance. From these two sets of short-range measurements in the anechoic chamber, we can confirm the suitability of treating the plywood board covered with light diffusers as a model impedance plane.

We also use the measured excess attenuation spectra in Fig. 8 to determine the acoustic impedances of the plywood board with (impedance façade surfaces) and without (hard ground surfaces) the cover of light diffusers. Attenborough's two-parameter model[25] was used to characterize the surface impedances, Z, of the vertical wall and the ground in the present study. The surface impedance is calculated by

$$Z = 0.538\sqrt{\sigma_e/f} + i[0.538\sqrt{\sigma_e/f} + 19.74\alpha_e/f], \tag{38}$$

where f is the source frequency, σ_e is the effective flow resistivity, and α_e is the effective rate of change in porosity with depth. The parametric values of σ_e and α_e are deduced from the short-range propagation measurement over the surface.

The best-fit parametric values for σ_e and α_e were 80 kPa s m^{-2} and 450 m^{-1} for the vertical walls (plywood boards covered with light diffusers) and 80 000 kPa s m^{-2} and 50 m^{-1} for the ground made of the plywood board. These parametric values for different boundary surfaces used in the numerical simulations are summarized in Table I for the ease of reference. Figure 8 also shows typical predicted excess attenuation spectra for the propagation of sound above the vertical walls and the ground where their impedances are calculated by using Eq. (38) with the parametric values given in Table I.

For the image source model and the current integral formulation, the one-third octave band absorption coefficients (α) of the boundary surfaces are calculated from the measured impedance by[22]

$$\alpha = \left| \frac{Z-1}{Z+1} \right|^2. \tag{39}$$

Using the Attenborough two-parameter impedance model,[25] the absorption coefficients of the ground and vertical walls in one-third octave bands are calculated and listed in Table II.

In indoor measurements, a Renkus-Heinz PN 61 self-powered loudspeaker was used as the source and a "B&K" 4189 pre-polarized free-field 1/2 in. condenser microphone was used as the receiver. A PC-based maximum length sequence system analyzer (Ref. 26) was used as both signal generator for the source and data analyzer of the measurements. The source strength was characterized by conducting prior measurements to measure its SPL at 1 m free field in the anechoic chamber. In the present indoor experiments, we presented the results for steady-state SPLs at various horizontal distances at different frequency bands. The source was located at 0.545 m away from the left vertical wall and at heights varying between 0.10 and 2.1 m. For the receiver, it was also situated at 0.545 m from the left vertical wall and 0.2 m above the ground.

Figure 9 shows the typical spectra of the steady-state SPLs where the receiver was located at 2 and 4 m from the source. The source and received were, respectively, placed at 0.6 and 0.2 m above the ground and at the same distance of 0.545 m from the left vertical wall. In the graphs, we compare the measured spectra with the numerical predictions according to the integral formulation. The measured and nu-

TABLE I. The best-fit parametric values of the effective flow resistivity (σ_e) and the effective rate of change in porosity with depth (α_e) for predicting the acoustic impedance of the boundary surfaces used in the indoor and outdoor experiments.

	σ_e (kPa s m^{-2})	α_e (m^{-1})
Indoor façade	80	450
Indoor ground	80 000	50
Outdoor façade	50 000	500
Outdoor ground	200 000	500

TABLE II. The estimated mean absorption coefficients of the boundary surfaces given in dB and the absorption coefficient of air at 30 °C and 80% relative humidity given in dB/km.

Frequency (Hz)	400	500	630	800	1000	1250	1600	2000	2500	3150	4000	5000	6300	8000
Absorption coefficient (indoor façade)	0.07	0.09	0.11	0.14	0.18	0.21	0.25	0.29	0.32	0.34	0.36	0.37	0.36	0.35
Absorption coefficient (indoor ground)	0.026	0.028	0.032	0.036	0.04	0.045	0.05	0.056	0.062	0.07	0.079	0.088	0.098	0.11
Absorption coefficient (outdoor façade)	0.028	0.03	0.036	0.041	0.046	0.052	0.059	0.067	0.075	0.084	0.094	0.11	0.12	0.13
Absorption coefficient (outdoor ground)	0.011	0.013	0.014	0.016	0.018	0.020	0.023	0.026	0.028	0.032	0.036	0.04	0.045	0.05
Air absorption (30 °C, 80% R.H.) (dB/km)	1.98	2.79	4.14	5.66	7.41	9.28	11.2	13.3	15.7	18.8	23.1	29.7	39.8	55.7

merical predictions agree reasonably well with each other except for one or two individual one-third octave bands, e.g., a discrepancy of about 5 dB was found for 3150 Hz in the 2 m separation and about 7 dB for 5 kHz in the 4 m separation. It is also observed that the integral formulation can predict the general trend of the measured spectral SPLs. The average discrepancies in the one-third octave bands were found to be 1.9 and 2.7 dB, respectively, for the 2 and 4 m separations.

The variation of the steady-state SPL with the horizontal separation is shown in Fig. 10 where four sets of typical results for the frequencies of 500 Hz, 1.25 kHz, 2.5 kHz, and 5 kHz are presented. The relative source/receiver positions with the ground and with the vertical walls are the same as in Fig. 9. These plots serve to highlight the capability of the integral formulation in predicting the general trend of measured data for the indoor model experiments.

Before we end this section, they wish to point out that there were other studies[26,27] examining an improved technique for simultaneously selecting both an optimal scale factor and optimal model materials for use in indoor scale model experiments. However, there is no attempt to select the most appropriate materials for modeling the façade surfaces in the present study. The use of a model impedance plane is sufficient to validate the integral formulation by comparing its predicted SPLs with the precise indoor measurements.[28]

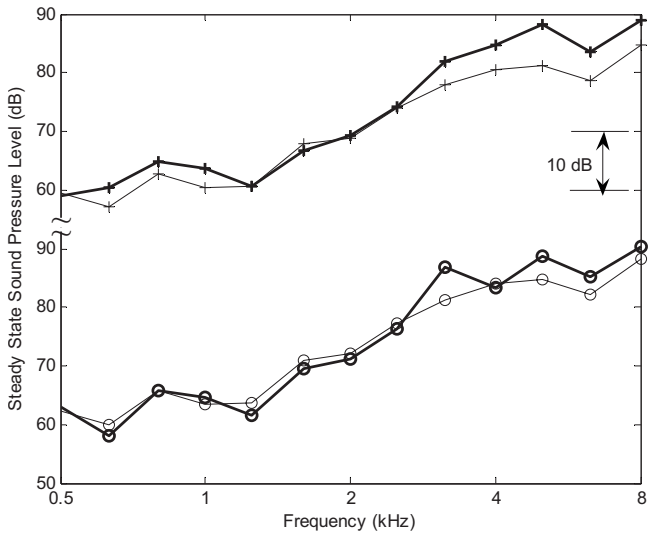

FIG. 9. The SPL spectra for the indoor model experiments. The source was located at 0.6 m above the ground and at 0.565 m from one side of the vertical wall. The receiver was placed at 0.2 m above the ground and 0.215 from the same wall. The thick solid lines are experimental data and the thin solid lines are predictions by the integral formulations. The lines with open circles and plus signs are for the horizontal separations of 2 and 4 m, respectively.

C. Outdoor field measurements in an alley street

To confirm the versatility of the integral formulation, we conducted a further set of full scale field measurements in an alley street. It was 3.13 m wide, 20 m long, and the height of the two parallel was 54 m. The alley street had a concrete ground and both vertical walls were covered with hard mosaic tiles. We used the same set of instrument for all indoor and outdoor measurements. Figure 11 shows the experimental setup in the alley street. In the experiments, the source was located at the center of the alley street and 0.1 m above the ground. The receiver was placed at a height of 1.6 m above the ground and at 0.69 m from one of the vertical walls. The distance between source and receiver was adjusted between 1 and 20 m.

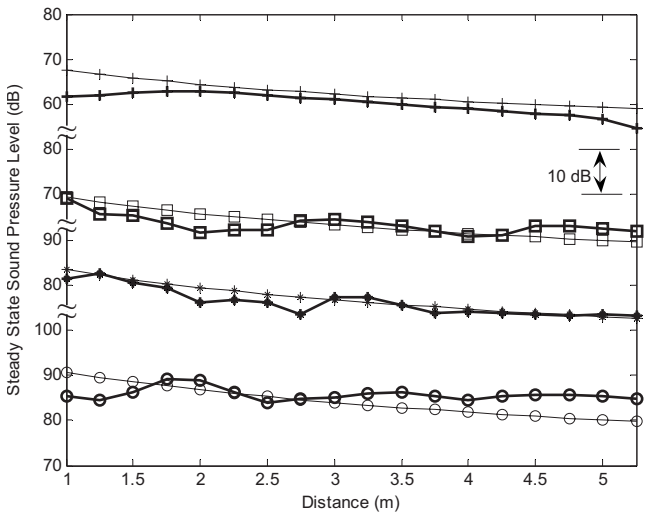

FIG. 10. The SPL is plotted versus the horizontal distance. The source and receiver locations are the same as Fig. 9. The thick solid lines are for experimental data and thin solid lines are for predictions by the integral formulation. (Plus signs: 500 Hz, squares: 1.25 kHz, asterisks: 2.5 kHz, and open circles: 5 kHz.)

FIG. 11. (Color online) Photograph showing the experiment setup of the field measurements in an alley street.

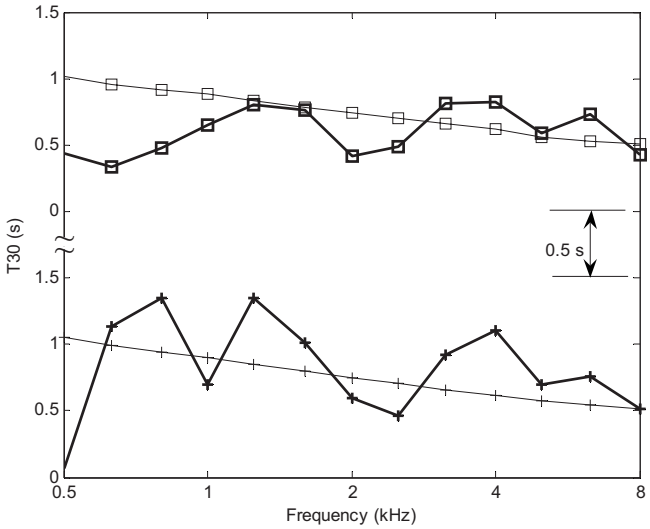

FIG. 12. The reverberation time T_{30} is plotted versus the source frequency where the source is placed at 0.1 m above the ground and at 1.56 m from one side of the vertical wall. The receiver was located at 1.6 m above the ground and 0.69 from the same vertical wall. The thick solid lines are for experimental data and thin solid lines are for predictions by the integral formulation. (Plus signs: source/receiver separation of 4 m and squares: source/receiver separation of 12 m.)

Prior *in-situ* measurements were conducted to determine the sound absorption coefficient of the vertical walls and the ground. The source and receiver were placed at 0.01 m above the respective surfaces and their horizontal separation was set at 1 m in these measurements. Again, the Attenborough two-parameter impedance model[25] was used to characterize the respective impedances of the surfaces and their parametric values are listed in Table I. All these boundary surfaces were made of acoustically hard construction materials, which led to fairly high parametric values for σ_e according to the short-range characterization measurements.

The sound absorption coefficients of the concrete ground and the vertical walls covered with mosaic tiles can then be calculated according to Eq. (39). These absorption coefficients, which are listed in Table II, will then be used in subsequent calculations of the reverberation times and SPLs in the alley street.

During the measurement, the outdoor temperature was about 30 °C and the relative humidity was 80%, the air absorption factors which are used in the following predictions and are obtained from Ref. 20. The air absorption coefficients at different frequency bands are listed in Table II. Due to the relatively high background noise levels in the field measurements, the reverberation time T_{30} was measured in favor of T_{60}. The SPL of the loudspeaker was measured at 1 m free field in the anechoic chamber before the field measurements. It was used to compare with the SPLs measured in the alley street.

Figure 12 shows the experimental data of T_{30} in one-third octave bands for the source and receiver located along the alley street. We compare the measured data with the numerical predictions of reverberation times for horizontal separations of 4 and 12 m. The numerical results according to the integral formulations are also shown in Fig. 12. We remark that the numerical predictions can only give a reasonable estimation of the general trend of T_{30} as the source frequency increases. Comparison of results for other source/receiver separations was generally similar to those shown in Fig. 12 but they are not shown here for succinctness. In this set of data, the source and receiver are placed at respective heights of 0.1 and 1.6 m above the ground. They are located at respective distances of 1.56 and 0.69 m from one of the vertical walls.

Figure 13 displays the variations of reverberation times with the horizontal separation. The source/receiver positions relative to the vertical walls and the ground are the same as above. Numerical results and measured data are presented for the source frequencies of 800 Hz, 1.6 kHz, 2 kHz, and 4 kHz. Similar results are also obtained for other frequencies but only four frequencies are selected for presentation. As shown in the plots, the predicted T_{30} varies marginally along the horizontal range (up to 15 m) although the experimental

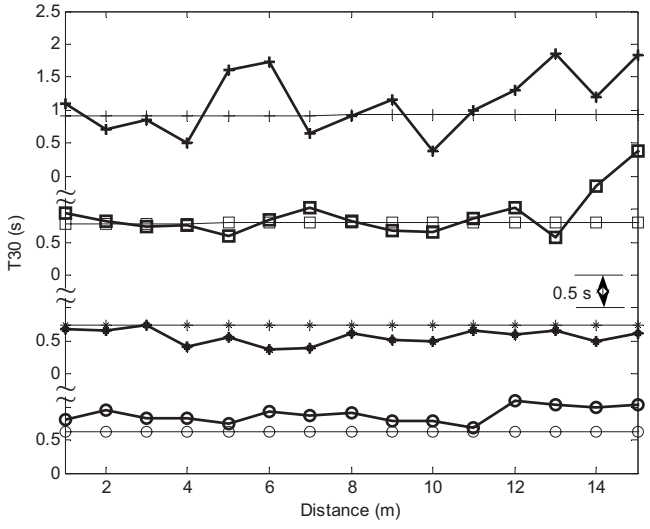

FIG. 13. The reverberation time T_{30} is plotted versus the distance. The source and receiver have the same relative positions from the vertical walls and the ground as described in Fig. 12. The thick solid lines are for experimental data and thin solid lines are for predictions by the integral formulation. (Plus signs: 800 Hz, squares: 1.6 kHz, asterisks: 2 kHz, and open circles: 4 kHz.)

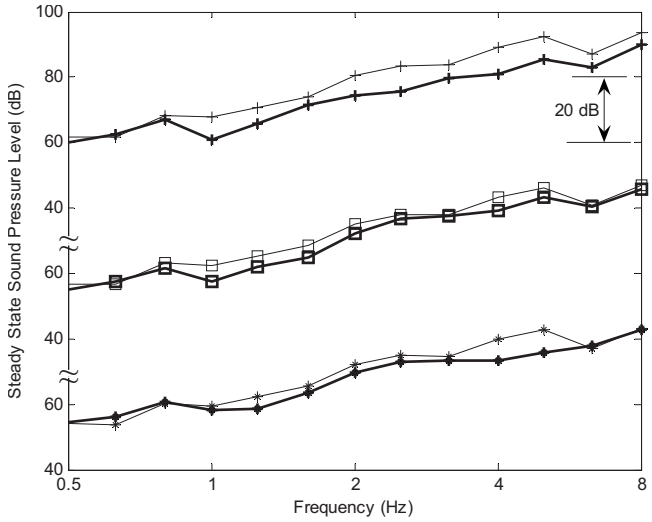

FIG. 14. The steady-state SPL is plotted versus the source frequency with the same source/receiver geometry as Fig. 12. The thick solid lines are for experimental data and thin solid lines are for predictions by the integral formulation. The respective source/receiver separations are 4 (plus signs), 12 (squares), and 20 m (asterisks).

data show a fluctuation in T_{30}. In general, the integral formulation can predict the average level of measured T_{30} over the range of interest.

Next, the same source/receiver geometries as above are used for the next two sets of the experimental measurements. In the first set of data, the predicted and measured spectra for the steady-state SPLs are compared in Fig. 14 for the respective horizontal separations of 4, 12, and 20 m. Apparently, the numerical predictions according to the integral formulation give reasonably good agreements with the general trends of the measured frequency spectra in all cases. In the second set of data, the variations of steady-state SPLs with the horizontal range were shown in Fig. 15 for the respective frequencies of 500 Hz, 800 Hz, 2 kHz, and 4 kHz. Again, the predicted results show tolerably good agreements with the general trend for the reduction in the SPLs when the separation between the source and receiver increases.

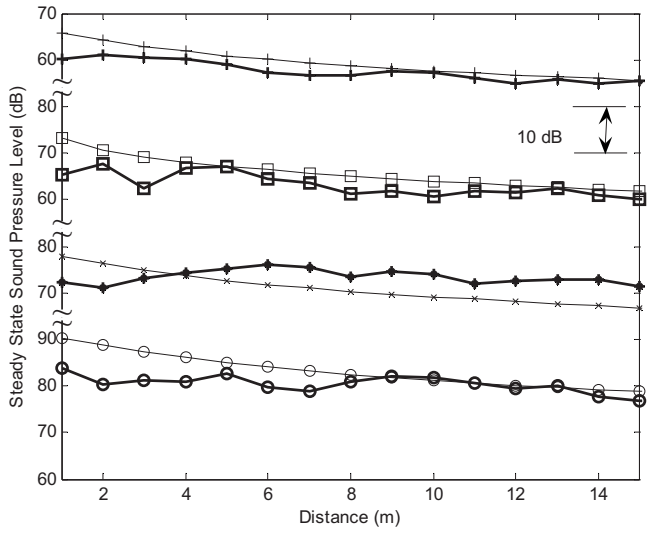

FIG. 15. The steady-state SPL is plotted versus the distance. The source/receiver geometry is same as Fig. 13. The thick solid lines are for experimental data and thin solid lines are for predictions by the integral formulation. (Plus signs: 500 Hz, squares: 800 Hz, asterisks: 2 kHz, and open circles: 4 kHz.)

IV. CONCLUSIONS

By modeling a street canyon as a long enclosure with an open top, it is possible to use an energy approach to sum the contribution from all image sources incoherently. In the present study, an integral formulation has been developed to estimate the noise levels in a street canyon by replacing the discrete image sources with an effective line source. The integral formulation is used to predict the decay curve of sound energy where the reverberation time in the street canyon can be estimated. Based on the reverberation time, the steady-state SPLs in the street canyon can be calculated. It has been demonstrated that the predictions according to the integral formulation agreed reasonably well with published data conducted in a town street. The numerical results according to the integral formulation also show good agreements with indoor and outdoor experimental data obtained in the present study. The integral formulation can be used to provide an efficient model for predicting noise levels and the reverberation effect in a street canyon.

ACKNOWLEDGMENTS

We are grateful to S. T. So, William Fung, and T. L. Yip for their help in conducting the outdoor and indoor experiments reported in this study. We are grateful to the three anonymous reviewers for their helpful comments.

[1]C. H. Chew, "Prediction of traffic noise from expressways—Part 1: Buildings flanking one side of expressways," Appl. Acoust. **28**, 203–212 (1989).
[2]C. H. Chew, "Prediction of traffic noise from expressway—Part II: Buildings flanking both sides of expressways," Appl. Acoust. **32**, 61–72 (1991).
[3]K. K. Chin, K. Y. Ng, S. K. Soon, and H. T. Chui, "A study of urban traffic noise," Proceedings Western Pacific Regional Acoustics Conference **2**, 142–145 (1997).
[4]K. M. Li, "Managing environment noise in Hong Kong," J. Acoust. Soc. Am. **115**, 2593 (2002).
[5]J. E. Volkmann and M. L. Graham, "A survey on air raid alarm signals," J. Acoust. Soc. Am. **14**, 1–9 (1942).
[6]L. M. Ball, "Air raid siren field tests," J. Acoust. Soc. Am. **14**, 10–13 (1942).
[7]F. W. Wiener, C. I. Malme, and C. C. Gogos, "Sound propagation in urban areas," J. Acoust. Soc. Am. **37**, 738–747 (1965).
[8]D. Aylor, J. Y. Parlange, and C. Chapman, "Reverberation in a city street," J. Acoust. Soc. Am. **54**, 1754–1757 (1973).
[9]K. W. Yeow, "External reverberation times observed in built-up area," J. Sound Vib. **48**, 438–440 (1976).
[10]K. W. Yeow, "Decay of sound levels with distance from a steady source observed in a built-up area," J. Sound Vib. **52**, 151–154 (1977).
[11]N. W. M. Ko and C. P. Tang, "Reverberation time in a high-rise city," J. Sound Vib. **56**, 459–461 (1978).
[12]P. Steenackers, H. Myncke, and A. Cops, "Reverberation in town streets," Acustica **40**, 115–119 (1978).
[13]R. H. Lyon, "Roles of multiple reflections and reverberation in urban noise propagation," J. Acoust. Soc. Am. **55**, 493–503 (1974).
[14]H. G. Davies, "Multiple-reflection diffuse-scattering model for noise propagation in streets," J. Acoust. Soc. Am. **64**, 517–521 (1978).
[15]J. Picaut, L. Simon, and J. Hardy, "Sound field modeling in streets with a diffusion equation," J. Acoust. Soc. Am. **106**, 2638–2645 (1999).
[16]J. Kang, "Sound propagation in street canyons: Comparison between diffusely and geometrically reflecting boundaries," J. Acoust. Soc. Am. **107**, 1394–1404 (2000).

[17]J. B. Allen and D. A. Berkley, "Image method for efficiently simulating small room acoustics," J. Acoust. Soc. Am. **65**, 943–950 (1979).
[18]K. K. Lu and K. M. Li, "The propagation of sound in narrow street canyons," J. Acoust. Soc. Am. **112**, 537–550 (2002).
[19]J. Kang, "Numerical modeling of the sound fields in urban streets with diffusely reflecting boundaries," J. Sound Vib. **258**, 793–813 (2002).
[20]"Method for calculation of the absorption of sound by the atmosphere," American National Standards Institute S1.26 (1995).
[21]M. Abramowitz and I. A. Stegun, *Handbook of Mathematical Functions, With Formulas, Graphs and Mathematical Tables* (Wiley, New York, 1972), Chap. 5.
[22]K. M. Li and P. M. Lam, "Prediction of reverberation time and speech transmission index in long enclosures," J. Acoust. Soc. Am. **117**, 3716–3726 (2005).
[23]M. R. Schroeder, "New method of measuring reverberation time," J. Acoust. Soc. Am. **37**, 409–412 (1965).
[24]G. A. Daigle, M. R. Stinson, and D. I. Havelock, "Experiments on surface waves over a model impedance plane using acoustical pulses," J. Acoust. Soc. Am. **99**, 1993–2005 (1996).
[25]K. Attenborough, "Ground parameter information for propagation modeling," J. Acoust. Soc. Am. **92**, 418–427 (1992).
[26]D. D. Rife and J. Van der Kooy, "Transfer-function measurement with maximum-length sequences," J. Audio Eng. Soc. **37**, 419–443 (1989).
[27]T. A. Busch and M. R. Hodgson, "Improved method for selecting scale factors and model materials for scale modelling of outdoor sound propagation," J. Sound Vib. **243**, 173–181 (2001).
[28]K. V. Horoshenkov, D. C. Hothersall, and S. E. Mercy, "Scale modelling of sound propagation in a city street canyon," J. Sound Vib. **223**, 795–819 (1999).